Lattice dynamics of cobalt-deficient CoO from first principles

U. D. Wdowik* and K. Parlinski
Institute of Technology, Pedagogical University, PL-30-084 Cracow, ul. Podchorazych 2, Poland
(Received 19 June 2008; revised manuscript received 28 November 2008; published 31 December 2008)

Ab initio calculated Hellmann-Feynman forces were used to investigate an influence of vacancies on the lattice dynamics of a charge-transfer insulator CoO. Electron correlations were taken into account by applying the Hubbard potential U and the exchange interaction J. Vacancies of concentrations of 3% and 6% were introduced into the cobalt sublattice. For structures with defects the phonon density of states and the phonon-dispersion relations were calculated. Vacancies influence predominantly the optical phonon vibrations. The increasing nonstoichiometry decreases the TO frequencies and increases the LO frequencies, while the long-wavelength acoustic phonons do not experience changes. The mean-squared vibrational amplitudes of both cobalt and oxygen increase with the increasing concentration of cobalt vacancies. Results of the calculations are compared to the existing experimental data.

DOI: 10.1103/PhysRevB.78.224114 PACS number(s): 61.72.−y, 63.20.kp, 63.20.dk

I. INTRODUCTION

Point defects (vacancies and impurities) can directly affect various features of the materials. Therefore, a good understanding of the host-matrix properties modified due to the incorporated defects is desired. On the other hand, experimental methods are very often unable to determine precisely some electronic and dynamical quantities of compounds which experience changes upon the point defect implementation.

Electronic structure and magnetic properties of simple 3*d* transition-metal oxides (NiO, CoO, FeO, and MnO) have been extensively studied by *ab initio* methods and most of these investigations were devoted to defect-free systems.[1–4] Calculations performed for defected NiO and MnO crystals indicate a vacancy-induced half metallicity of these compounds.[5] Electronic structure of cation-deficient CoO has been a subject of *ab initio* calculations as well.[6] It was found that cation vacancies are responsible for the creation of trivalent cobalt ions within the CoO lattice. Trivalent cations arise from the charge-transfer process which converts initial divalent cobalt to trivalent state. Trivalent cobalt ions introduce acceptor states into the band gap of the CoO matrix.

An *ab initio* method could be used to study an influence of the point defects, such as cation vacancies, on the lattice dynamics. Such theoretical investigations employed to strongly correlated systems are a challenging research subject. For these systems the complicated electronic structure, extensive ionic relaxations, and electronic structure modifications in the presence of vacancies are still demanding tasks for *ab initio* methods. Moreover, the difficulties arise also from the highly correlated nature of electron interactions, namely, strong on-site Coulomb repulsions between 3*d* electrons, which govern both the electronic structure and lattice dynamics of the 3*d* transition-metal oxides.[7–9]

Typically, in the density-functional theory, interactions between correlated states are described by the Hubbard energy U and the Hund local exchange interaction J.[1,2] Using appropriate U and J terms, one could predict the correct ground state of the stoichiometric CoO and properly describe the vibrational properties of its lattice.[10]

The phonon calculations of CoO with $U=0$ eV and $J=0$ eV are unsuccessful. An approach which neglects on-site interactions leads to an appearance of metallic ground state of the CoO crystal and unphysical imaginary phonon frequencies. These soft modes indicate that a metallic state of CoO is not a ground state of this crystal. Such artificial modes arise from the underestimated Hellmann-Feynman (HF) forces when no repulsion in the 3*d* shell allows the charge to flow freely. The presence of the soft modes disables to compute any phonon-dependent thermodynamical functions due to the negative values of the phonon density of states. Note that for a metallic state no LO-TO splitting exists.

Paramagnetic CoO has the NaCl-type crystal structure (space group $Fm\bar{3}m$) with a lattice constant of 4.2614 Å (Ref. 11) and becomes antiferromagnetically ordered below the Néel temperature of about 291 K. Cobalt oxide exhibits a second kind of antiferromagnetic ordering (AFII), i.e., the magnetic structure consists of ferromagnetic (111) sheets with adjacent planes having opposite spin directions.[12,13] The spin-up and spin-down cobalt ions constitute two ferromagnetic sublattices, and hence the AFII supercell is twice as large as the crystallographic *fcc* unit cell. At the onset of magnetic ordering, CoO experiences a small tetragonal distortion ($c/a=0.988$) which is accompanied by a rhombohedral distortion[11] with the angle of the pseudocubic cell of 89.962°. Density-functional theory corrected for the strong electron correlations indicates that, in the ground state, CoO is a charge-transfer insulator[14] with the experimental energy-band gap of about 2.5–2.8 eV.[15]

In general, CoO is a nonstoichiometric metal-deficient oxide.[16,17] The cobalt deficiency depends on temperature and external oxygen partial pressure. There are practically no cobalt interstitials and the oxygen sublattice is almost perfectly ordered.[18] The concentration of cobalt vacancies ranges from 0.1% to 3%.[19] Vacancies are believed to stay in uncharged or charged state.[16] Uncharged Co vacancies are accompanied by trivalent cobalt ions. Therefore, a defect electronic band can be composed of trivalent Co ions, uncharged Co vacancies, and singly and doubly charged cobalt vacancies. Uncharged vacancies are able to accept up to two electrons. Trivalent

cobalt ions and uncharged vacancies are acceptors, doubly charged vacancies are donors, while singly charged vacancies can be either acceptors or donors. On the other hand, CoO is able to accommodate a variety of trivalent impurities which are likely to associate strongly with their charge compensating cation vacancies.[20]

The paper is aimed at the study of an influence of point defects such as cationic vacancies on the lattice dynamics of charge-transfer insulator CoO. It is expected that the vibrational dynamics of the nonstoichiometric lattice may be different from the dynamics of the perfect lattice. This is an attempt to study the lattice dynamics of a real system containing some imperfections. The present computational study may stimulate further theoretical and experimental investigations in this research field.

II. COMPUTATIONAL DETAILS

A supercell approach was used to model a nonstoichiometric CoO containing cobalt vacancies. One has to note that, within such approach, calculation of low defect concentrations is still limited to a few percent.

The AFII supercell of the defect-free CoO (space group $R\bar{3}m$) contains 64 atoms. The spin-up and spin-down sublattices are symmetric and distinguished from each other only with respect to the orientation of cobalt magnetic moments. Hence, no sublattice is preferred to create a vacancy and introducing one vacancy into the first or to the second sublattice having the reversed spin direction gives the same effect.

A neutral vacancy was created by removing one Co atom having fractional coordinates of $(\frac{1}{2}\frac{1}{2}\frac{1}{2})$ from the AFII supercell. Since we use a supercell concept, the concentration of periodically distributed vacancies leads to the nonstoichiometric oxide $Co_{0.97}O$. The crystal $Co_{0.94}O$ with a doubled vacancy concentration was constructed in the similar manner. Two neutral Co atoms located at $(\frac{1}{2}\frac{1}{2}\frac{1}{2})$ and $(\frac{1}{2}\frac{1}{2}0)$ positions of the AFII supercell were removed. These vacancies are separated by a crystallographic lattice constant and reside in the ferromagnetic sublattices having opposite spin orientations. The $Co_{0.94}O$ supercell has both cationic sublattices equally defected and the spin-up and spin-down ferromagnetic sublattices are symmetric. The majority-spin component on one cobalt sublattice is the minority-spin component on the other cobalt sublattice. CoO crystals with 3.125% and 6.250% vacancy concentrations, denoted further as 3% and 6%, were represented by supercells consisting of 63 and 62 atoms, respectively. Two primitive cells containing 31 atoms each build up the $Co_{0.94}O$ supercell. The $Co_{0.97}O$ and $Co_{0.94}O$ structures contain 12 and 13 crystallographically nonequivalent atoms, respectively.

Calculations have been performed using the plane wave basis VASP code[21] which implements spin-polarized density-functional theory. Atoms were represented by projector-augmented wave pseudopotentials (PAWs).[22] The valence electrons of cobalt and oxygen were described by the potential configurations $(3d^8 4s^1)$ and $(2s^2 2p^4)$, respectively. Gradient-corrected exchange-correlation functional PW91 (Ref. 23) was used and the plane waves were expanded up to energies of 520 eV. Effects of electron correlation beyond generalized gradient approximation (GGA) were taken into account within the framework of GGA+U and the simplified (rotationally invariant) approach of Dudarev *et al.*[2] The Coulomb repulsion $U=7.1$ eV and the local exchange interaction $J=1$ eV were applied to describe the on-site interactions in the cobalt $3d$ shell. These values lead to the energy gap for undefected CoO of 2.77 eV,[10] which stays in a good agreement with the experimental energy gap of 2.5–2.8 eV.[15] It should be noted that supercell optimizations were performed for U ranging from 1 to 9.1 eV and with $J=1$ eV. The lattice constant shows a weak dependence on U, in contrast to the energy gap, which is very sensitive to the choice of U.[10] All energies U, which are smaller than 5 eV, considerably underestimate the energy gap. The energy $U=1$ eV corresponds to the GGA limit at which the energy gap vanishes and CoO becomes a metal. The magnetic moment behaves smoothly versus U and changes by $\sim 17\%$ throughout the entire U range, reaching $2.74\mu_B$ for $U=7.1$ eV.[10] Comparing the lattice constant, magnetic moment, and the energy gap of CoO with the available theoretical and experimental data, one finds $U=7.1$ eV as the most appropriate value to be used in further detailed calculations. It should be noted that $U=7.8$ eV and $J=0.78$ eV were obtained by Anisimov *et al.*[1] When $U=7.1$ eV is applied, the calculated phonon-dispersion curves for defect-free CoO reproduce the inelastic neutron-scattering data[24] with a reasonable accuracy.

The Brillouin zone was sampled using $2\times2\times2$ k-point mesh generated by the Monkhorst-Pack scheme.[25] A combination of conjugate gradient energy minimization and a quasi-Newton force minimization was used to optimize geometry and the atomic positions of the supercell. The forces acting on each atom of the supercell were minimized down to 10^{-5} eV/Å, while the differences in the total energies between two successive electronic iterations were required to be less than 10^{-7} eV.

The phonon-dispersion relations and the vibrational density of states for each nonstoichiometric system have been calculated within the harmonic approximation and by using the direct method[26,27] based on the forces calculated via Hellmann-Feynman theorem. The nonvanishing HF forces $F_i(n,\mu)$ acting on the atoms (n,μ) in the supercell are generated when a single atom (m,ν) is displaced from its equilibrium position. The following relation between the displacements $u_j(m,\nu)$ and the forces $F_i(n,\mu)$ applies:

$$F_i(n,\mu) = -\sum_j \Phi_{ij}(n,\mu,m,\nu)u_j(m,\nu), \tag{1}$$

where $\Phi_{ij}(n,\mu,m,\nu)$ are the force constants. Taking into account the crystal symmetry, $\Phi_{ij}(n,\mu,m,\nu)$ are fitted to the HF forces by singular value decomposition algorithm. Those force constants are used to construct the dynamical matrix of the system, $\mathbf{D}(\mathbf{k})$, which depends on the wave vector $\mathbf{k}$. Diagonalization of $\mathbf{D}(\mathbf{k})$,

$$\omega^2(\mathbf{k},j)\mathbf{e}(\mathbf{k},j) = \mathbf{D}(\mathbf{k})\mathbf{e}(\mathbf{k},j), \tag{2}$$

leads to the eigenvalues $\omega(\mathbf{k},j)$ and the eigenvectors $\mathbf{e}(\mathbf{k},j)$, which represent the frequencies and polarization vectors of phonons, respectively. Here, the mode index j distinguishes

between the phonon branches at the given wave vector **k**.

For ionic and covalent crystals, the splitting between transverse-optic (TO) and longitudinal-optic (LO) modes due to the coupling between atomic displacements and a long-range macroscopic electric field is calculated via the nonanalytical term added to the dynamical matrix.[28] The nonanalytical contribution depends on the Born effective charge tensor and the high-frequency dielectric constant ϵ_∞.

The partial phonon density of states describes the contribution to the density of states for the selected atom μ vibrating along a selected Cartesian coordinate i. It is defined as

$$g_{i,\mu}(\omega) = \frac{1}{nd\Delta\omega}\sum_{\mathbf{k},j} |e_i(\mathbf{k},j;\mu)|^2 \delta_{\Delta\omega}(\omega - \omega(\mathbf{k},j)), \quad (3)$$

where $e_i(\mathbf{k},j;\mu)$ is the ith Cartesian component of the eigenvector of the mode $(\mathbf{k},j)$ for the atom μ, $\Delta\omega$ denotes the frequency interval, n is the number of sampling wave-vector points, d stands for the dimension of $\mathbf{D}(\mathbf{k})$, while $\delta_{\Delta\omega}(x)$ equals 1 if $|x| \leq \Delta/2$; otherwise, it is equal zero. The total vibrational density of states can be obtained as $g(\omega) = \Sigma_{i,\mu} g_{i,\mu}(\omega)$.

In the present calculations, the HF forces were generated by displacing each crystallographically nonequivalent atom from its equilibrium position by 0.03 Å in all three Cartesian directions. Both positive and negative displacements were applied to minimize the systematic errors. The number of calculated displacements was equal to 72 and 78 for structures with 3% and 6% vacancy concentrations, respectively.

The Born effective charges for cobalt and oxygen $|Z^*| = 2.06$ have been adopted from Ref. 10. They have been estimated for stoichiometric CoO using the $q \to 0$ limit technique and the Lyddane-Sachs-Teller relation $\omega_{\mathrm{LO}}^2 - \omega_{\mathrm{TO}}^2 \sim |Z^*|^2/\epsilon_\infty$, taking $\epsilon_\infty = 5.3$ from Ref. 29, experimental $\omega_{\mathrm{LO}} = 15.75$ THz from Ref. 24, and the calculated $\omega_{\mathrm{TO}} = 10.25$ THz.

III. RESULTS AND DISCUSSION

In the present paper we limit our consideration to harmonic phonons. A typical approach to lattice dynamics makes use of the periodic symmetry of a crystal, so that the phonon modes are given within the primitive unit cell. By solving the dynamical matrix $\mathbf{D}(\mathbf{k})$ one obtains $3N$ phonon-dispersion curves, where N is the number of atoms in the primitive unit cell. It is worthwhile to stress that a selection of the primitive unit cell as a crystalline unit is a convention. One may select a larger crystal unit cell, being a multiplication of the primitive one, and call such a cell a supercell. There are several consequences of such a selection: (i) the dimensions of the dynamical matrix increase to three times the number of atoms in the supercell, (ii) the number of phonon-dispersion curves increases correspondingly, and (iii) the size of a new Brillouin zone conjugated with the supercell shrinks. For example, the primitive unit cell of CoO contains two atoms, while the supercell of $2\times2\times2$ size of the crystallographic unit cell consists of $2\times2\times2\times4\times2 = 64$ atoms, where 4 stands for the volume increase from the crystallographic to primitive cubic unit cell. Therefore, a new Brillouin zone shrinks and for such Brillouin zone the number of phonon-dispersion curves is raised to 192. Since this new Brillouin zone is also periodic and fills the reciprocal space, it would mean that, by a simple selection of a different kind of a unit cell, we blow up the number of phonon-dispersion curves. This is, of course, not true, as there are only six phonon-dispersion curves in the whole reciprocal space. The above discussion does not take into account the phonon form factor, which enters any scattering experiment. This form factor determines whether a given mode is a real and observable phonon mode or is a fake mode which is experimentally never seen. The simplest form factor has the following form:

$$F^{(p)}(\mathbf{k},j) = \frac{1}{\mathbf{k}^2}\left|\sum_\mu \frac{\mathbf{k}\cdot\mathbf{e}(\mathbf{k},j;\mu)}{\sqrt{M_\mu}}\right|^2, \quad (4)$$

where M_μ is the mass of the μth atom involved in the j phonon branch at the wave vector **k**. The form factor $F^{(p)}(\mathbf{k},j)$ occurs in the dynamical structure factor which defines the intensity of one-phonon coherent neutron or x-ray scattering. For all fake phonons, $F^{(p)}(\mathbf{k},j) = 0$.

One may ask about the advantage of the description of phonon modes within a supercell. The advantage can be seen immediately if one inserts into a supercell a point defect, e.g., a vacancy. Then, the symmetry of the original crystal lowers and the supercell becomes a primitive unit cell. This means that the original symmetry is broken and some fake phonon modes may become visible. It is an important effect. Those arisen modes, i.e., fake modes which exhibit now the nonvanishing intensities, carry on an information on the defect and the defect's surrounding vibrations. It is known that point defects, even in the harmonic approximation, affect the phonon vibrations, and therefore an appearance of the additional modes reflects an influence of the point defect, including a vacancy, on the lattice dynamics.

For general discussion the form factor [Eq. (4)] is not always the most convenient since its value depends on the crystal orientation with respect to the momentum transfer. A more convenient quantity, called here a *filter*, which indicates the real occupation of the phonon branches, can be obtained by averaging the form factor (4) over all possible relative orientations between **k** and $\mathbf{e}(\mathbf{k},j;\mu)$. This averaging denoted by $d\Omega$ leads to the following expression:

$$\int_\Omega d\Omega\, F^{(p)}(\mathbf{k},j) = \frac{1}{3}F^{(s)}(\mathbf{k},j), \quad (5)$$

where $F^{(s)}(\mathbf{k},j)$ has the following form:[27]

$$F^{(s)}(\mathbf{k},j) = \left|\sum_\mu \frac{\mathbf{e}(\mathbf{k},j;\mu)}{\sqrt{M_\mu}}\right|^2. \quad (6)$$

Filter $F^{(s)}(\mathbf{k},j)$ represents an intensity of a given phonon mode and allows to estimate the relative intensities of all modes across a variety of Brillouin zones. It is able to remove most of the unessential phonon branches carrying very low intensities. A filtering procedure is not so unusual. It has been already used in elaboration of the molecular-dynamics simulation of crystalline ammonia.[30]

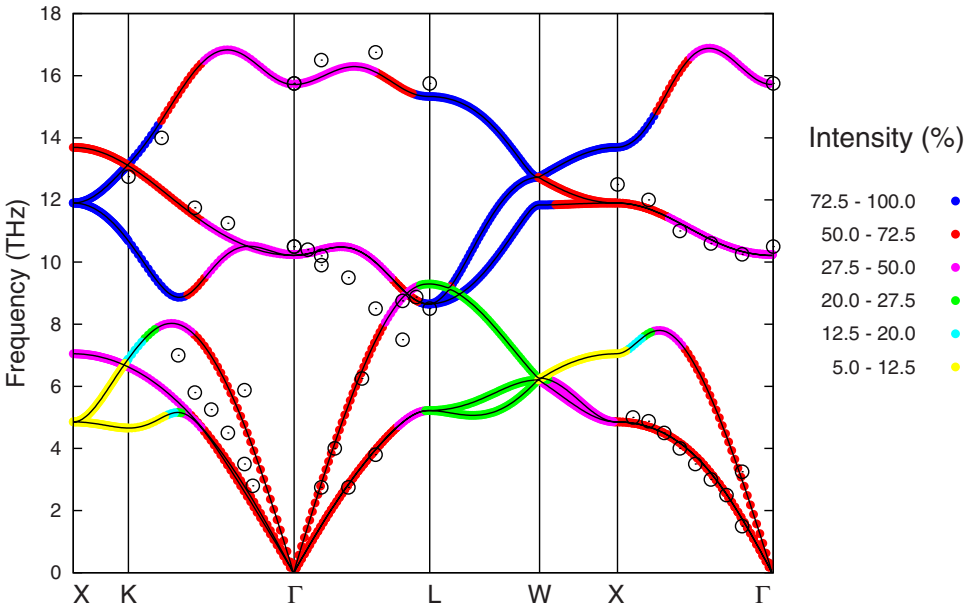

FIG. 1. (Color online) Phonon-dispersion relations for stoichiometric CoO obtained from *ab initio* calculations in Ref. 10 (thin solid line), experimental data measured by inelastic neutron scattering in Ref. 24 (open symbols), and dispersion curves intensities (color symbols given in the legend). The legend gives the linear scale of the intensity determined by the filter [Eq. (6)] for each phonon mode. 100% was assigned to the most intense phonon mode. The modes with intensities below 5% are not shown. The high-symmetry points are labeled according to fcc Brillouin zone of the cubic phase.

Here, the perfect CoO shows six phonon branches.[10] The supercells for $Co_{0.97}O$ and $Co_{0.94}O$ have $N=63$ and $N=31$ atoms, and therefore they exhibit 189 and 93 phonon branches, respectively. All phonon-dispersion curves are drawn in reciprocal space to which we have adopted the notation of high-symmetry points from fcc Brillouin zone.

The phonon-dispersion relations along high-symmetry directions of the Brillouin zone for the stoichiometric CoO are shown in Fig. 1. The low-temperature (110 K) data obtained by the inelastic neutron scattering[24] are shown for comparison as well. The infrared-active mode splits to $\omega_{TO}=10.25$ THz and $\omega_{LO}=15.75$ THz. The frequency ω_{TO} is very close to the experimentally determined values of 10.50 THz (Ref. 24) and 10.40 THz.[29]

The filter proposed above [Eq. (6)] was applied to defect-free CoO and the resulted intensities of the normal modes are shown in Fig. 1. Maximal value of $F^{(s)}(\mathbf{k},j)$, which corresponds to the highest intensity, was set to 100%. It can be seen in Fig. 1 that neutron-scattering data gather close to the branches having intensities higher than 30%.

For supercells with one and two vacancies, the phonon-dispersion relations, displayed using filter $F^{(s)}(\mathbf{k},j)$, are shown in Fig. 2 and Fig. 3, respectively. Only the modes having intensities higher than 5% are plotted. Some phonon branches show discontinuities which arise from the 5% cutoff of the applied filter. One has to notice that majority of phonon peaks is very weak in comparison to the intensity observed for the perfect CoO lattice. This could be understood as a manifestation of the broadening of phonon peaks due to the interaction with vacancies. The vacancies perturbing the lattice periodicity are natural obstacles for the phonon propagation throughout the lattice. Hence, perturbed are pre-

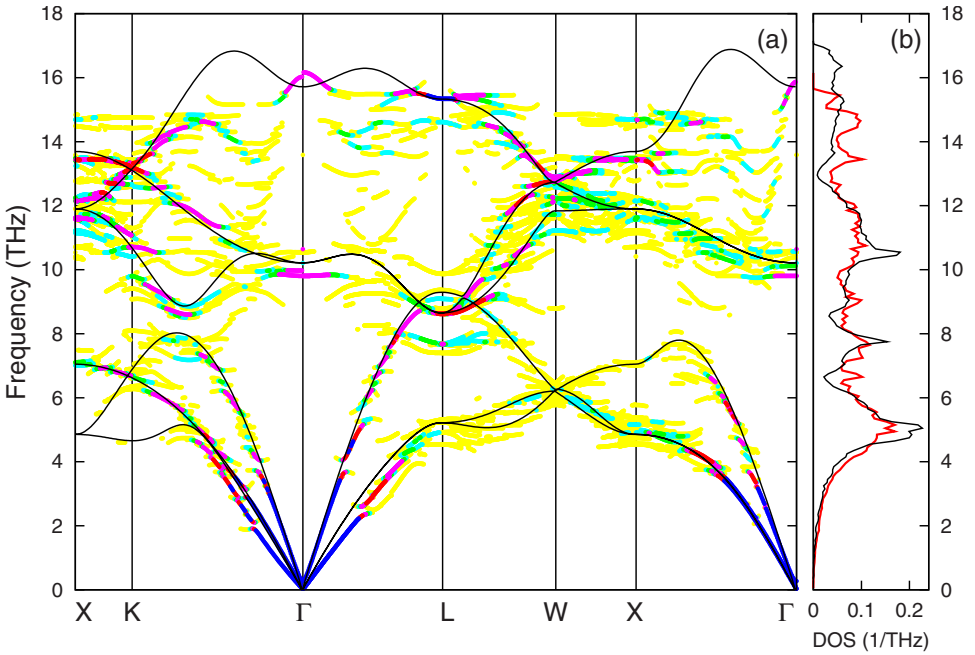

FIG. 2. (Color online) (a) Phonon-dispersion curves for $Co_{0.97}O$ shown as intensities defined by Eq. (6). See Fig. 1 for the legend. Phonon-dispersion relations for stoichiometric CoO obtained in Ref. 10 are shown for comparison as thin solid lines. (b) Phonon density of states for $Co_{0.97}O$ (color curve) and for stoichiometric CoO (black curve).

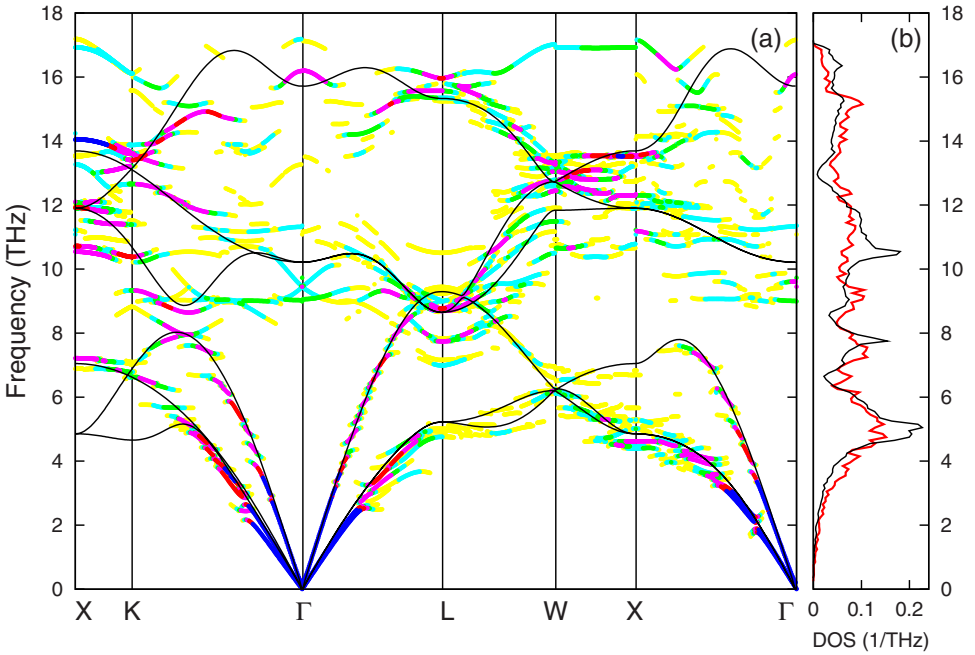

FIG. 3. (Color online) (a) Phonon-dispersion curves for $Co_{0.94}O$ shown as intensities defined by Eq. (6). See Fig. 1 for the legend. Phonon-dispersion relations for stoichiometric CoO obtained in Ref. 10 are shown for comparison as thin solid lines. (b) Phonon density of states for $Co_{0.94}O$ (color curve) and for stoichiometric CoO (black curve).

dominantly phonons with wavelengths comparable to the size of the region disturbed by the vacancy. These wavelengths correspond to the reciprocal lattice points *X*, *L*, and *W*. This effect would be smeared out if defects were distributed randomly.

The cobalt vacancy in CoO gives rise to an appearance of additional modes. Indeed, the oxygen atoms around the vacancies have less cobalt neighbors in the first coordination sphere, and hence the effective force constants are changed. These additional oxygen vibrations due to a smaller mass of oxygen are mainly located at the higher frequencies. It can be noticed in Figs. 2 and 3 that TO frequencies at Γ point decrease with an increase in vacancy concentration. For nonstoichiometric and perfect CoO the TO frequencies at the Brillouin-zone center are collected in Table I. The frequencies were estimated using the modes with intensities higher than 50%. Table I compares the estimated frequencies with the experimental data obtained from neutron scattering[24] and infrared-absorption spectroscopy.[29] Assuming that ϵ_∞ and $|Z^*|$ depend very weakly on the presence of vacancies, one may estimate the frequency of the LO mode and calculate the LO-TO splitting which amounts to 6.06 and 6.47 THz for $Co_{0.97}O$ and $Co_{0.94}O$, respectively.

The main contribution to the high-frequency part of the acoustic phonons comes from the cobalt sublattice, while the high-frequency optical phonons are dominated by the dynamics of the light oxygen atoms.[10] For small wave vectors, the acoustic branches of nonstoichiometric crystals remain sharp and stay very close to the acoustic branches of the vacancy-free crystal. Such a behavior is expected as the long-wavelength phonons are insensitive to point defects. Both transverse and longitudinal modes become broader while approaching the Brillouin-zone boundaries. For the structure with 3% vacancies the frequency smearing at the edges of the Brillouin zone reaches 1 THz while the crystal with 6% vacancies exhibits about 30% larger smearing.

Figure 4 shows the essential differences in the oxygen partial phonon densities of states. These densities were calculated according to Eq. (3) and they are due to the oxygen atoms being the nearest neighbors to the vacancy. They are compared to the partial phonon density of states of those oxygen atoms which surround the cobalt in the defect-free CoO. It can be seen that vacancies affect mostly the spectra of the highest frequencies belonging to the longitudinal-optic modes. The oxygen atoms surrounding defects are found to introduce to the density of states much more high-frequency modes as compared to the fully coordinated ions. No significant change in the phonon density of states of the low-frequency acoustic region is observed.

Knowledge of the phonon density of states allows us to establish thermodynamic functions. For example, the heat capacity at low temperatures can be affected by the presence

TABLE I. Γ-point optical frequencies (ω_{TO} and ω_{LO}) for nonstoichiometric and stoichiometric CoO. The static dielectric constant ϵ_∞=5.3 and the Born effective charges $|Z^*|$=2.06 were taken to calculate ω_{LO}. Theoretical results for stoichiometric CoO are adopted from Ref. 10.

	Theoretical			Neutron scattering	Infrared spectroscopy
	CoO	$Co_{0.97}O$	$Co_{0.94}O$	Ref. 24	Ref. 29
ω_{TO} (THz)	10.25	9.81	9.61	10.50	10.40–10.49
ω_{LO} (THz)	15.73	15.87	16.08	15.75	16.30–16.40

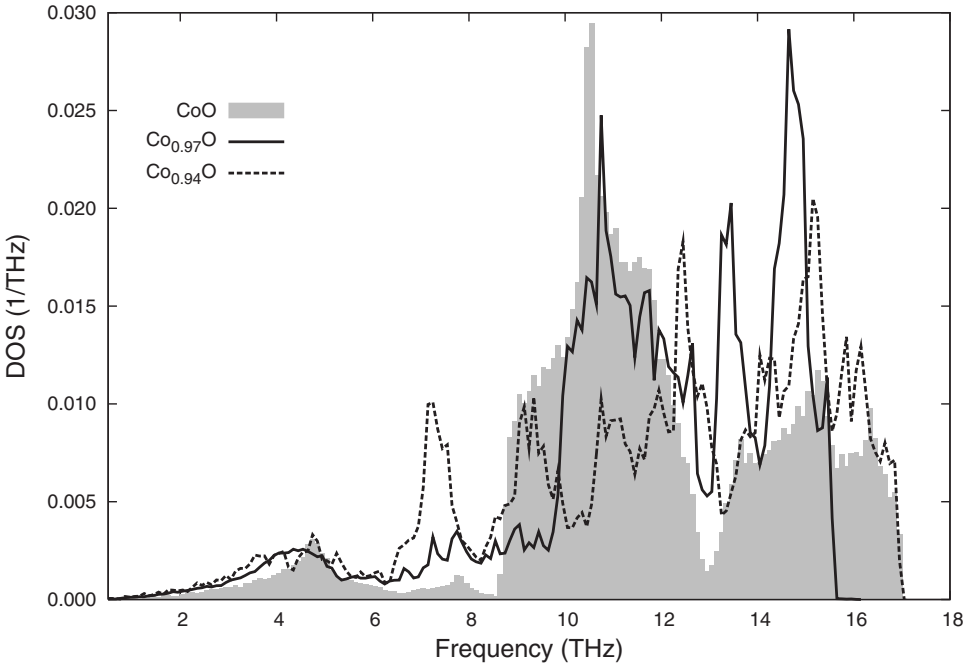

FIG. 4. Partial phonon density of states for oxygen atoms surrounding the vacancy in $Co_{0.97}O$ (solid curve), $Co_{0.94}O$ (dotted curve), and fully coordinated cobalt in CoO (shaded area). The partial densities of states have been calculated according to Eq. (3).

of vacancies. One should remember however that at low temperatures the heat capacity of CoO is dominated by a magnetic contribution.[31]

A diffraction scattering intensity contains the Debye-Waller factor defined as $\exp\{-W_\mu(\mathbf{k})\}$, where

$$W_\mu(\mathbf{k}) = \frac{1}{2}[2\pi\mathbf{k}\cdot\mathbf{B}(\mu)\cdot(2\pi\mathbf{k})]. \quad (7)$$

$\mathbf{B}(\mu)$ represents the static correlation function of displacement $U(\mu)$ of the μth atom from its equilibrium position and it is a second-rank symmetric tensor having the following components:

$$B_{ij}(\mu) = \langle U_i(\mu)U_j(\mu)\rangle. \quad (8)$$

$\mathbf{B}(\mu)$ represents the mean-squared displacement (MSD) of the atom μ and it is expressed by the diagonal and off-diagonal partial phonon densities of states $g_{il,\mu}(\omega)$ taking on the following form:[27]

$$B_{il}(\mu) = \frac{\hbar r}{2M_\mu}\int_0^\infty d\omega\, g_{il,\mu}(\omega)\omega^{-1}\coth\left(\frac{\hbar\omega}{2k_BT}\right), \quad (9)$$

where $\hbar$ is the Planck's constant, k_B denotes the Boltzmann constant, and T is the temperature. Symbols M_μ and r denote the mass of the atom μ and the number of degrees of freedom in the primitive unit cell, respectively.

The average mean-squared amplitude of atomic vibrations versus temperature is shown for stoichiometric and nonstoichiometric CoO in Fig. 5. Calculations are compared to MSD determined by Γ-ray[11] and x-ray[32] experiments. The x-ray data are significantly higher than the Γ-ray data and our theoretical results. It was suggested[11] that either the lack of thermal diffusive scattering or the monochromator applied could account for the observed discrepancy. In the entire temperature and stoichiometry ranges, cobalt atoms show lower vibrational amplitudes as compared to oxygen atoms, reflecting the mass difference between cobalt and oxygen. At low temperatures both constituents of the defected lattices show about 5% larger vibrational amplitudes as compared to the MSD of the perfect lattice constituents (see Table II for details). On the other hand, the difference in MSD between structures containing 3% and 6% vacancies is negligible at low temperatures and it becomes more significant at elevated temperatures. The MSD increases with the increasing nons-

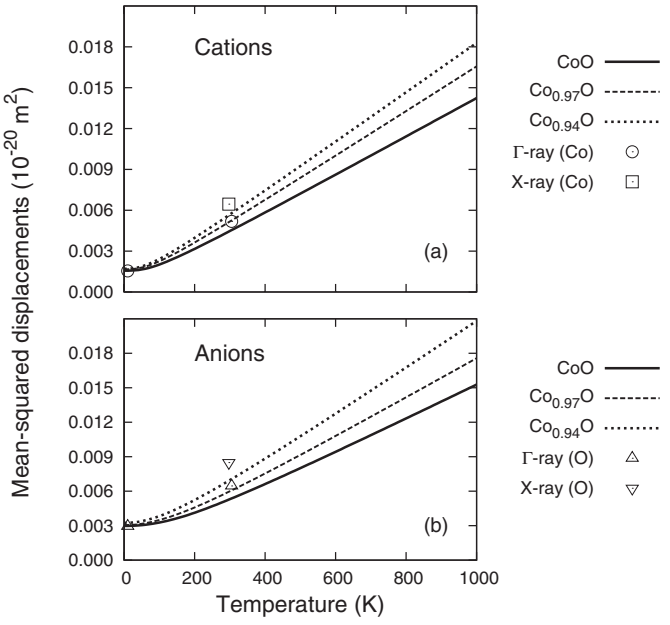

FIG. 5. Mean-squared displacements vs temperature for cobalt and oxygen atoms in stoichiometric and nonstoichiometric CoO. Solid, dashed, and dotted curves correspond to CoO, $Co_{0.97}O$, and $Co_{0.94}O$, respectively. The Γ-ray data (Ref. 11) are shown as open circles and up triangles for cations and anions, respectively. X-ray data (Ref. 32) are denoted by open squares and down triangles for cations and anions, respectively.

TABLE II. Theoretical and experimental (Ref. 11) averaged mean-squared vibrational amplitudes and their slopes at elevated temperatures for cobalt and oxygen atoms in stoichiometric and nonstoichiometric CoO. MSD is given in ($Å^2 \times 10^{-2}$) while its slope is given in ($Å^2 \times 10^{-5}$/K).

	CoO		$Co_{0.97}O$		$Co_{0.94}O$		Expt. (Ref. 11)	
MSD	10 K	305 K	10 K	305 K	10 K	305 K	10 K	305 K
Co	0.157	0.452	0.164	0.508	0.166	0.543	0.148(7)	0.518(2)
O	0.298	0.534	0.314	0.616	0.317	0.634	0.291(30)	0.645(11)
MSD slopes at elevated temperatures								
Co	1.399		1.584		1.702			
O	1.429		1.701		1.761			

toichiometry and temperature. For cations and anions the change in MSD with the increasing temperature is given in Table II by the respective MSD slopes calculated for temperatures exceeding 300 K. Vibrational amplitudes of cobalt atoms in $Co_{0.97}O$ and $Co_{0.94}O$ are 13% and 22% higher than those experienced in stoichiometric CoO. The oxygen moves more freely giving the increase in MSD of 19% and 23% for structures with 3% and 6% vacancies, respectively. The mean-squared displacements of ions being more distant from the vacancy saturate to the MSD values corresponding to the ideal crystal sublattices.

IV. SUMMARY

A supercell approach was used to model a structure of CoO crystal containing vacancies. The lattice dynamics of CoO with 3% and 6% cation vacancies has been studied within the harmonic approximation and by the direct method. The phonon density of states and the phonon-dispersion relations were obtained for $Co_{0.97}O$ and $Co_{0.94}O$. They were compared to those obtained for stoichiometric CoO. To analyze the numerous phonon-dispersion curves, a filter which enables to remove the fake phonon branches was applied. It allowed us to present the phonon-dispersion curves to be more close to the dispersion relations of a real defected sample.

Vacancies influence primarily the optical phonon region, while the long-wavelength acoustic phonons are practically not affected by defects. Therefore, a small concentration of defects does not disturb those crystal properties which are due to the low-frequency acoustic phonons. The slight softening of TO modes and hardening of LO modes with increasing nonstoichiometry are observed. The optical phonon band of structures with vacancies is much more broadly distributed than the respective band of a perfect structure. Oxygen atoms surrounding vacancy experience larger MSD than the respective ions having the saturated bond. The average mean-squared vibrational amplitudes of the ions constituting particular sublattices of CoO increase with the increasing vacancy concentration. The intensity of the scattered radiation from the defected structure decreases due to the lower values of the Debye-Waller factors.

One has to note that the present calculations are done for a crystal with quite high vacancy concentrations. Therefore, a signal from such a system can be enhanced as compared to the signal from nearly stoichiometric sample. For low vacancy concentrations the signal from defects is possibly hidden in the experimental spectra of CoO, and hence further experimental verification is required.

ACKNOWLEDGMENTS

The authors would like to thank P. Piekarz for valuable comments. This work was supported by the Polish Ministry of Scientific Research (MNiSW) Grant No. 3T11F 031 29. Interdisciplinary Modeling Center (ICM), Warsaw University, Poland is acknowledged for providing the computer facilities under Grant No. G28-12.

*Corresponding author. FAX: +48126372243; sfwdowik@cyf-kr.edu.pl

[1] V. I. Anisimov, J. Zaanen, and O. K. Andersen, Phys. Rev. B **44**, 943 (1991); V. I. Anisimov, I. V. Solovyev, M. A. Korotin, M. T. Czyzyk, and G. A Sawatzky, *ibid.* **48**, 16929 (1993).

[2] S. L. Dudarev, G. A. Botton, S. Y. Savrasov, C. J. Humphreys, and A. P. Sutton, Phys. Rev. B **57**, 1505 (1998).

[3] A. Svane and O. Gunnarsson, Phys. Rev. Lett. **65**, 1148 (1990).

[4] Z. Szotek, W. M. Temmerman, and H. Winter, Phys. Rev. B **47**, 4029 (1993).

[5] D. Ködderitzsch, W. Hergert, Z. Szotek, and W. M. Temmerman, Phys. Rev. B **68**, 125114 (2003).

[6] U. D. Wdowik and K. Parlinski, Phys. Rev. B **77**, 115110 (2008).

[7] S. Y. Savrasov and G. Kotliar, Phys. Rev. Lett. **90**, 056401 (2003).

[8] S. L. Dudarev, L. M. Peng, S. Y. Savrasov, and J. M. Zuo, Phys. Rev. B **61**, 2506 (2000).

[9] S. Massidda, M. Posternak, A. Baldereschi, and R. Resta, Phys. Rev. Lett. **82**, 430 (1999).

[10] U. D. Wdowik and K. Parlinski, Phys. Rev. B **75**, 104306 (2007).
[11] W. Jauch, M. Reehuis, H. J. Bleif, F. Kubanek, and P. Pattison, Phys. Rev. B **64**, 052102 (2001); W. Jauch and M. Reehuis, *ibid.* **65**, 125111 (2002).
[12] W. L. Roth, Phys. Rev. **110**, 1333 (1958); C. G. Shull, W. A. Strauser, and O. Wollan, *ibid.* **83**, 333 (1951); D. Herrmann-Ronzaud, P. Barlet, and J. Rossat-Mignod, J. Phys. C **11**, 2123 (1978).
[13] B. Morosin, Phys. Rev. B **1**, 236 (1970); L. C. Bartel and B. Morosin, Phys. Rev. B **3**, 1039 (1971); B. T. M. Willis and H. P. Rooksby, Acta Crystallogr. **6**, 827 (1953).
[14] G. A. Sawatzky and J. W. Allen, Phys. Rev. Lett. **53**, 2339 (1984); J. Zaanen, G. A. Sawatzky, and J. W. Allen, *ibid.* **55**, 418 (1985).
[15] J. van Elp, J. L. Wieland, H. Eskes, P. Kuiper, G. A. Sawatzky, F. M. F. de Groot, and T. S. Turner, Phys. Rev. B **44**, 6090 (1991); R. J. Powell and W. E. Spicer, *ibid.* **2**, 2182 (1970).
[16] J. Nowotny, I. Sikora, and M. Rekas, J. Electrochem. Soc. **131**, 94 (1984); E. Fryt, Oxid. Met. **10**, 311 (1976).
[17] M. Schroeder and M. Martin, Z. Phys. Chem. **207**, 1 (1998); G. Borchardt, K. Kowalski, J. Nowotny, M. Rekas, and W. Weppner, J. Mater. Sci. **31**, 5185 (1996).
[18] R. Dieckman, Z. Phys. Chem., Neue Folge **107**, 189 (1977).
[19] K. Persels Constant, T. O. Mason, S. J. Rothman, and J. L. Routbort, J. Phys. Chem. Solids **53**, 405 (1992); K. Hoshino and N. L. Peterson, *ibid.* **45**, 963 (1984).
[20] R. W. Grimes and S. P. Chen, J. Phys. Chem. Solids **61**, 1263 (2000).
[21] G. Kresse and J. Furthmüller, computer code VASP, Vienna, Austria, 1999; G. Kresse and J. Furthmüller, Comput. Mater. Sci. **6**, 15 (1996); G. Kresse and J. Hafner, Phys. Rev. B **47**, 558 (1993); G. Kresse and J. Furthmüller, *ibid.* **54**, 11169 (1996).
[22] P. E. Blöchl, Phys. Rev. B **50**, 17953 (1994).
[23] J. P. Perdew, J. A. Chevary, S. H. Vosko, K. A. Jackson, M. R. Pederson, D. J. Singh, and C. Fiolhais, Phys. Rev. B **46**, 6671 (1992).
[24] J. Sakurai, W. J. L. Buyers, R. A. Cowley, and G. Dolling, Phys. Rev. **167**, 510 (1968).
[25] H. J. Monkhorst and J. D. Pack, Phys. Rev. B **13**, 5188 (1976).
[26] K. Parlinski, Z-.Q. Li, and Y. Kawazoe, Phys. Rev. Lett. **78**, 4063 (1997).
[27] K. Parlinski, software PHONON, Cracow, 2008.
[28] R. M. Pick, M. H. Cohen, and R. M. Martin, Phys. Rev. B **1**, 910 (1970).
[29] P. J. Gielisse, J. N. Plendl, L. C. Mansur, R. Marshall, S. S. Mitra, R. Mikolajewicz, and A. Smakula, J. Appl. Phys. **36**, 2446 (1965).
[30] M. M. Siddick, G. J. Ackland, and C. A. Morrison, J. Chem. Phys. **125**, 064707 (2006).
[31] E. G. King and A. U. Christensen, U. S. Bur. Mines Tech. Paper **80**, 1800 (1956); E. G. King, *ibid.* **80**, 2399 (1956); E. N. Abarra, K. Takano, F. Hellman, and A. E. Berkowitz, Phys. Rev. Lett. **77**, 3451 (1996).
[32] S. Sasaki, F. Fujino, and Y. Takeuchi, Proc. Jpn. Acad., Ser. B: Phys. Biol. Sci. **55**, 43 (1979).